Measurement Science and Technology

100 year anniversary
Measurement Science and Technology

PAPER

Validation of low-cost ozone measurement instruments suitable for use in an air-quality monitoring network

To cite this article: David E Williams *et al* 2013 *Meas. Sci. Technol.* **24** 065803

Meas. Sci. Technol. **24** (2013) 065803 (12pp) doi:10.1088/0957-0233/24/6/065803

Validation of low-cost ozone measurement instruments suitable for use in an air-quality monitoring network

David E Williams[1], Geoff S Henshaw[2], Mark Bart[2], Greer Laing[2], John Wagner[2], Simon Naisbitt[2] and Jennifer A Salmond[3]

[1] MacDiarmid Institute for Advanced Materials and Nanotechnology, School of Chemical Sciences, University of Auckland, Private Bag 92019, Auckland 1142, New Zealand
[2] Aeroqual Ltd, 109 Valley Rd, Mt Eden, Auckland, New Zealand
[3] School of Environment, University of Auckland, Private Bag 92019, Auckland 1142, New Zealand

E-mail: david.williams@auckland.ac.nz, geoff.henshaw@aeroqual.com, mark.bart@aeroqual.com and j.salmond@auckland.ac.nz

Received 8 December 2012, in final form 3 April 2013
Published 3 May 2013
Online at stacks.iop.org/MST/24/065803

Abstract
This paper presents a novel low-cost instrument that uses a sensor based on conductivity changes of heated tungstic oxide, which is capable of accurately measuring ambient concentrations of ozone. A combination of temperature steps and air flow-rate steps is used to continually reset and re-zero the sensor. A two-stage calibration procedure is presented, in which a nonlinear transformation converts sensor resistance to a signal linear in ozone concentration, then a linear correlation is used to align the calibration with a reference instrument. The required calibration functions specific for the sensor, and control system for air flow rate and sensor temperature, are housed with the sensor in a compact, simple-to-exchange assembly. The instrument can be operated on solar power and uses cell phone technology to enable monitoring in remote locations. Data from field trials are presented here to demonstrate that both the accuracy and the stability of the instrument over periods of months are within a few parts-per-billion by volume. We show that common failure modes can be detected through measurement of signals available from the instrument. The combination of long-term stability, self-diagnosis, and simple, inexpensive repair means that the cost of operation and calibration of the instruments is significantly reduced in comparison with traditional reference instrumentation. These instruments enable the economical construction and operation of ozone monitoring networks of accuracy, time resolution and spatial density sufficient to resolve the local gradients that are characteristic of urban air pollution.

Keywords: ozone, instrumentation, networks

(Some figures may appear in colour only in the online journal)

1. Introduction

Air quality is inherently variable in time and space, concerns every individual and impacts directly on health and productivity [1]. Ozone (O_3) is a significant atmospheric pollutant, which has both an acute and chronic impact on human health at concentrations as low as 70 μg m^{-3} measured as an 8 h average (35 parts-per-billion (ppb) by volume) [2]. O_3 is also known to damage vegetation both in pristine and agricultural environments [3], with the probability and extent of damage increasing with mean concentration [4]. Ozone is formed as a secondary pollutant in the troposphere as a result of the photo-dissociation of nitrogen dioxide (NO_2), which itself is primarily formed by reactions of the exhaust emissions of internal combustion engines (nitric oxide and unburnt hydrocarbons). High concentrations

of O_3 are therefore typically found downwind of large conurbations or industrial sources. Ultraviolet light is necessary for the production of O_3, so concentrations typically peak in the mid-afternoon. However, O_3 is also rapidly depleted in the atmosphere as a result of reactions with other pollutants such as nitric oxide, and readily decomposed on surfaces. This means that in urban areas concentrations are highly variable, peaking in areas away from traffic but dropping to near zero close to immediate sources of primary pollutants especially overnight. Large diurnal cycles in concentration result, the characteristics of which may vary considerably in space [5–8].

Measurements of O_3 distribution and hence modelling of the large spatial and temporal variations in O_3 concentrations required in order to understand effects of this pollutant on health and the environment have been limited by the instrumentation available. Conventional (spectroscopic) instruments are bulky, expensive and require ac power, temperature-controlled enclosures, and weekly or often daily calibration. These considerations limit their deployment in the field both in terms of the number of instruments and choice of monitoring site and create questions of resource allocation [9–11]. The resulting networks of regulatory instruments may not adequately resolve the strong gradients in vertical and horizontal pollutant concentration [12] which are significant for assessment of personal exposure [2, 13] and the identification of health or environmental impacts [1, 14–17]. Further, limited data availability hinders the identification of robust relations between O_3 and meteorological variables [18] and transport pathways in remote inaccessible environments, hindering attempts to understand and predict pollutant transport pathways [19]. Such limitations have led to attempts to deduce the pollutant burden and consequent health effects [20, 21] from measurement of traffic density, emission inventories and dispersion modelling [22–26] and by various correlation [27–30] and computational techniques [16, 20, 31–39]. It would be more reliable, however, to increase the spatial density of measurement instruments so that interpolation is less uncertain [40, 41]. There is therefore a need for the introduction of low-cost instruments which can easily be deployed in a high density network [42].

Semiconducting oxides have been intensively investigated as gas-sensitive resistor materials for ozone measurement, because the resistance response is large, the measurement is simple and the materials offer the possibility of mass-production sensor manufacture [43–59]. Various schemes of miniaturization have been explored, which typically utilize the kinetics of response of the material following a 'reset', either using temperature steps [60] or exposure to UV light [58, 59]. The challenge to overcome for atmosphere measurement network application is to sustain a reliable signal, without calibration, for long periods of time, with minimal, simple maintenance. This paper presents a novel low-cost instrument that uses a sensor based on conductivity changes of heated tungstic oxide and which is capable of measuring ambient concentrations of O_3. The instrument is a low powered device (∼1 W) which can be operated on solar power and has been successfully coupled with cell phone technology to enable monitoring in remote locations. Data from field trials are presented here to demonstrate not only the accuracy of the instrument but also the stability of the instrument over periods of months. We show that common failure modes can be detected through measurement of signals available from the instrument. The combination of long-term stability, self-diagnosis, and simple, inexpensive repair means that the cost of operation and calibration of the instruments is significantly reduced in comparison with spectroscopic reference instrumentation. The operation of networks with a density of monitoring instruments sufficient to resolve the intra-region and particularly intra-urban heterogeneity of O_3 concentrations, which results from meteorology, topography and variations in source strength of NO_2 and other pollutants that act to deplete concentrations or catalyse the production reactions [61], becomes feasible.

2. Instrument design strategy and construction

2.1. Background

Gas sensors based on conductivity changes of heated semiconducting oxides [53] are widely used for industrial safety monitoring. While there are reports in the literature of gas-sensitive resistors being used for ambient atmospheric monitoring, there is a perception that the devices suffer from effects such as drifts of zero and calibration slope, and cross-sensitivities to other gases making them unsuitable for quantitative, long-term atmosphere measurement. However, we have shown that with careful attention to detail these perceived deficiencies can be overcome [56, 57]. The very large conductance response at temperatures in the range 300–550 °C of highly porous layers of WO_3 to the introduction of ppb concentrations of ozone in air has been described and discussed in detail [54, 60, 62]. The design principles for instruments that utilize this effect and which compensate for sensor drift and for effects of variation in atmospheric relative humidity and of other interfering species have been presented elsewhere [60]. The sensor conductance can be partitioned into an ozone-independent term that represents the 'bulk' conductance, and an ozone-dependent term that represents the 'surface' conductance. The major effects causing drift of the signal were demonstrated to arise in the 'bulk' conductance term, and could be eliminated by a simple subtraction of the conductance in the presence of ozone from that in the absence of ozone. The method used is a combination of the sensor response to a temperature step and to an air flow-rate step. The response is slow so the purpose of the temperature step is to provide a well-defined initial state which is set up at the high temperature (typically 550–600 °C), so that the subsequent kinetics, at the low temperature after the step (typically 350–450 °C) are well defined [60]. Then, the conductance, σ, at any specific time after the step to low temperature is given by [60]

$$\sigma_{(O_3=0)} - \sigma = \frac{aP_{O_3}}{bP_{O_3} + 1}, \tag{1}$$

where the parameters a and b depend on the time after the step at which the measurement is made. Hence with $\Delta\sigma$ denoting

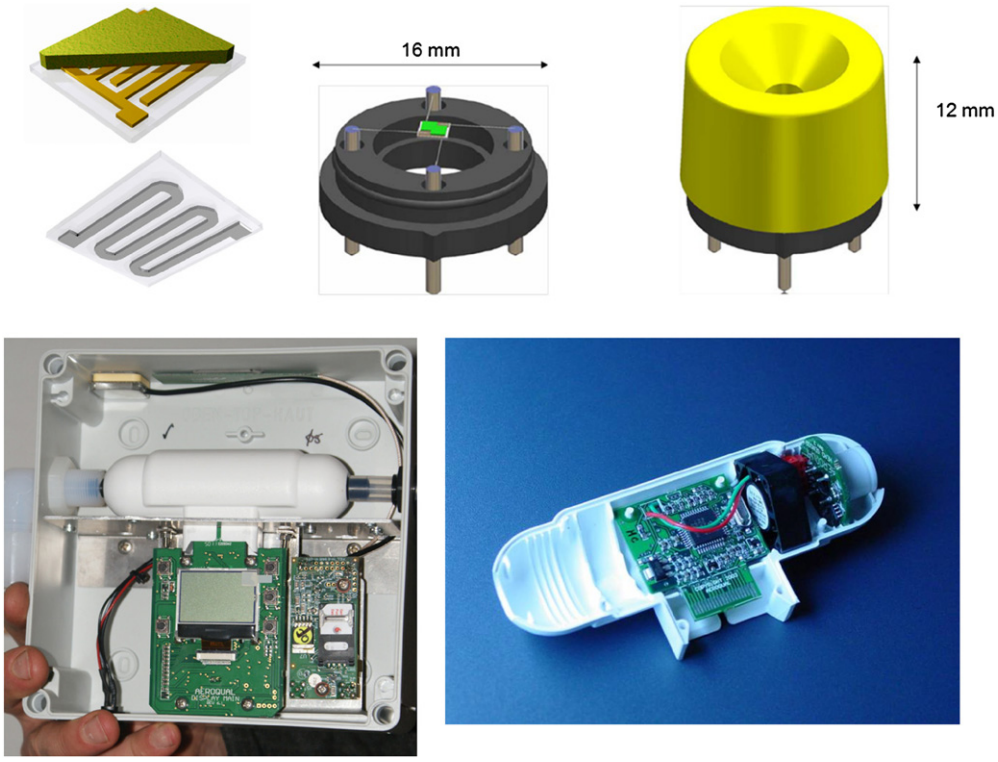

Figure 1. Sensor and instrument construction. The sensor (see text) is printed on an alumina tile, 2 mm square, mounted by fine Pt wires in a housing which directs onto the sensor an air flow, driven by a fan mounted on the base of the device. The head unit holds all the sensor-specific calibration information. The rest of the instrument handles data storage, presentation and communication.

the difference of conductance between the measured value in the atmosphere and the zero-ozone conductance

$$Po_3 = \left(\frac{\Delta\sigma}{a}\right)\left(1 - \frac{b\Delta\sigma}{a}\right)^{-1}. \quad (2)$$

For measurement over the ozone concentration ranges found in the atmosphere $b\Delta\sigma/a \ll 1$, so

$$Po_3 = \frac{1}{a}\Delta\sigma + \frac{b}{a^2}(\Delta\sigma)^2 + O(\Delta\sigma)^3. \quad (3)$$

Hence the ozone partial pressure can be estimated from the observed conductance difference with a simple quadratic, as previously noted [63] though a deviation from this simple relationship is expected at higher ozone concentration. Reference [53] showed the need for a sufficiently high flow rate directed at the sensor, to avoid the effect of the destruction of ozone on the warm plastic surfaces that surround the sensor. A sufficiently high flow rate can be achieved by machining a nozzle into the top of the sensor housing and drawing air through the housing by way of a hole centred directly under the sensor (figure 1). The other side of this effect is that the zero-ozone response required for application of equation (2) can elegantly be obtained simply by switching the flow through the sensor between a low and a high value [57, 60]. At a low flow rate, ozone is destroyed on the warm surfaces that surround the sensor. An alternative method is to switch the flow through an ozone destruction catalyst, but this is more bulky and more expensive to implement. One advantage of the flow switching method is that the 'zero' measurement is made in an atmosphere that is essentially the same as that in which the ozone measurement is made, so effects of water vapour and interferences, which are largely also additive in the conductance, cancel to a significant degree.

In practice, equation (1) is not exact. The degree to which the partitioning of the conductance into an ozone-sensitive 'surface' term and an ozone-insensitive 'bulk' term represents the behaviour of any individual sensor depends upon the microstructure. A second source of error in the application of the flow-switching method is that, at high ozone concentration full destruction of ozone might not be achieved so the zero ozone conductance estimate could be increasingly erroneous as the ozone concentration increases. We have overcome these issues by a two-stage calibration: first a linearization of the sensor output and then a final calibration.

2.2. Linearization

The first stage of the calibration is to measure the instrument response, $\Delta\sigma$, as a function of ozone concentration at a sufficient number of points to define a response function such as equations (2) or (3). The estimated ozone concentration derived from such fitting is P_{est}, a function of the measured conductance difference, $\Delta\sigma$, and the parameters of the fitting function (the coefficients a and b in equation (2), for example): $P_{\mathrm{est}} = f(\Delta\sigma, a, b)$. The estimating function would in general not be exact—it would be derived from a least-squares fit of the assumed response function to the calibration data. The parameters would themselves have an error estimate that reflected the goodness-of-fit and the data, $\Delta\sigma$, would

also be subject to some measurement error. Then for some subsequent measurement of an ozone concentration, actual value P_{O_3}, using the particular conductance difference, $\Delta\sigma$, the difference between the actual and estimated concentrations can be expressed as a Taylor series in a small variation of the parameters:

$$\Delta P = P_{O_3} - P_{\text{est}} \approx -\frac{\partial f}{\partial a}\delta a - \frac{\partial f}{\partial b}\delta b + O((\delta a)^2, (\delta b)^2) \quad \cdots \cdots \tag{4}$$

For the estimating function (2) above, we have

$$\Delta P \approx -P_{O_3}\left(\frac{\delta a}{a}(1 + bP_{O_3}) - \delta b P_{O_3}\right). \tag{5}$$

If the ozone concentration is small (that is bP_{O_3} and $\delta b P_{O_3} \ll 1$), then the leading error term is linear in the ozone concentration, so a linear, or at worst a quadratic correction can be derived to convert the estimated ozone concentration to the actual value. This analysis applies to any suitably chosen empirical fitting function that represents the data over the calibrated range.

2.3. Calibration

The estimating function (e.g. equation (2) or (3)) can be empirically adjusted to account for factors such as incomplete removal of ozone during the low-flow, zero-estimation phase of the measurement cycle. If the estimating function is correctly chosen then the linearization produces an estimated concentration, P_{est}, which is a linear function of the actual concentration, P_{O_3}. The second stage of the calibration procedure then is to estimate the correction ΔP to be applied to P_{est} using a least-squares linear fit of the dependence of P_{est} on P_{O_3} for a small number of calibrated values of P_{O_3}.

2.4. Instrument construction

The instrument (figure 1) is in two parts. A detachable head houses the sensor, fan or air pump, air inlet filters and sensor control electronics. The linearization function is loaded into this unit, which delivers a digitized, linearized output. The second part of the unit comprises the power, communications and display. Sensor construction is illustrated in figure 1(*a*). The device comprises a 2 × 2 × 0.250 mm alumina tile with a meandering platinum heater track printed on one side, and inter-digitated gold electrodes printed on the other. A thin (90 μm approx.) layer of WO_3 is screen printed over the gold electrodes, creating the sensing element. Alteration of print parameters such as particle size, firing temperature, ink loading and medium composition can be used to alter the sensitivity and thus adjust the sensor behaviour for different target concentration ranges. The sensor housing is a sealed cylindrical plastic enclosure with four bonding posts in the base from which the sensor is suspended freely in the air by fine platinum connecting wires. The pump draws air through the housing by an outlet directly beneath the sensor. The top of the housing is formed as a conical nozzle that directs air onto the face of the sensor element at a rate precisely controlled by the pump or fan. The nozzle dimensions and flow rates depend upon the sensor and housing dimensions and were empirically adjusted to achieve the desired performance. Precise control of the operating temperature is essential to instrument precision and stability, simply because the oxide conductivity varies strongly with temperature: the activation energy is about 0.5 eV. The method employed for temperature control incorporates the platinum heater track (which has a well-defined resistance–temperature relationship) into a Wheatstone bridge circuit whereby the out-of-balance signal across the two arms of the bridge is used to regulate the current through the sensor heater, thus controlling the heater temperature by keeping its resistance constant [63]. The measurement sequence is schematically illustrated in figure 2. The time for temperature stabilization at each step was a few seconds, as judged from the sensor resistance transient. The duration of each step was 30 s [60]. The sensor resistance is determined with a simple dc measurement, with the potential difference across the sensor controlled at 0.1 V. Higher potential differences across the sensor were found to cause an excessive resistance drift. The inlet air is drawn through a stainless steel mesh and a porous poly(tetrafluoroethylene)—PTFE—filter.

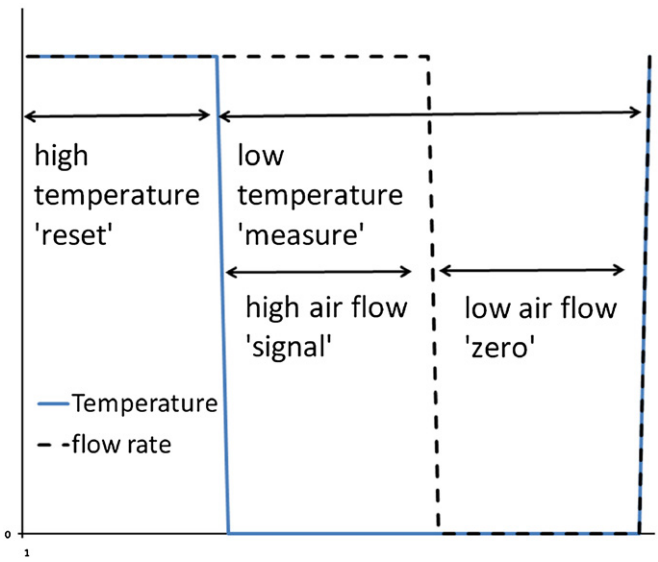

Figure 2. Sequence of temperature and air-flow steps used for the measurement.

2.5. Calibration procedure

The detachable heads are calibrated as complete units. The units are mounted in a rack inside a large Perspex box though which filtered ambient air (thus containing ozone dependent on ambient conditions) is drawn. The air inside the box is stirred by a fan. Ozone is generated inside the box by a controllable, shielded UV source. The air inside the box is sampled to a spectrometric reference analyser, that is itself periodically calibrated against standard instruments ultimately traceable to NIST, Washington DC. In the first stage of the procedure, linearization, the sensor resistance for each head is read at a sequence of increasing ozone concentration. The resistance is fitted to the linearization function and the parameters of

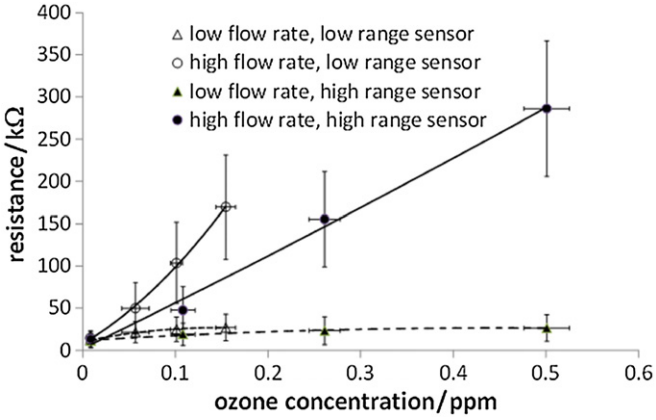

Figure 3. Sensor resistance response to variation of ozone concentration (parts-per-million, ppm, by volume) averaged over a large number of sensors. The ozone signal is derived at high air flow rate; the zero signal at low air flow rate. The sensor resistance is measured 5 s and 35 s after the high to low temperature step. The fan is turned off at the high temperature and is turned on immediately after the first low-temperature resistance measurement. The performance of sensors with microstructure optimized for two different concentration ranges of measurement is illustrated (low range: $N \sim 1000$; high range, $N \sim 2500$; mean resistance ± 1 population SD).

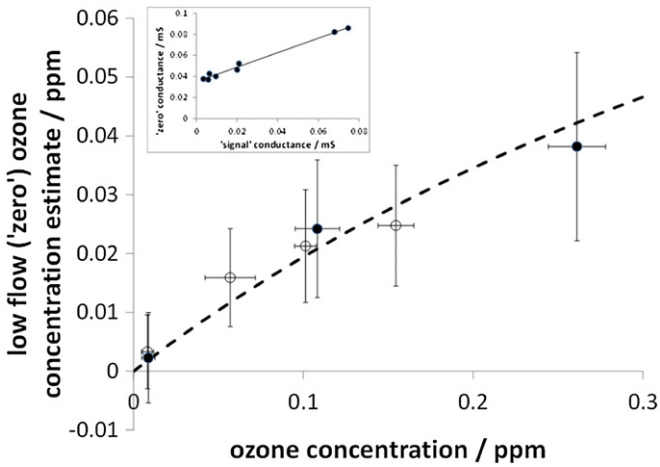

Figure 4. Ozone concentration present at the sensor in the low flow-rate ('zero') condition, estimated approximately by linear interpolation of the sensor resistance using the two lowest concentration points from the response curve presented in figure 2 Mean $\pm$ 1 population SD for low-range (open symbol, $N \sim 1000$) and high-range (closed symbol, $N \sim 2500$) devices. Inset: correlation between 'signal' conductance, measured at high flow rate, and 'zero' conductance, measured at low flow rate; mean results for all 3500 sensors. The dashed line is the fit to the concentration estimate assuming the observed linear correlation of conductances and equation (1) for the sensor response.

this function are loaded into the head. In the second stage, carried out independently, the ozone concentration in the box is again cycled and the linearized output from each head unit is compared to the reference analyser measurement.

3. Results and discussion

3.1. Linearization results

Figure 3 shows the sensor resistance dependence on ozone concentration, averaged over a large number of sensors. There is, as expected, variation between devices. One question is how well the low-flow condition approximates to a state of zero ozone concentration. The resistance variation at high flow-rate in the presence of ozone was used to estimate the ozone concentration present at the sensor in the low flow condition, by a simple linear interpolation between the resistance values for the two lowest ozone concentrations. The low-flow ('zero') ozone concentration present at the sensor was 10–20% of the actual ozone concentration (figure 4). The conductance of the sensor in the low flow state was on average linearly correlated with that in the high-flow state. The consequences for the drift compensation are discussed later.

Given the empirically observed linear relationship between the measured (low flow rate) 'zero', $\sigma_{0,m}$, and the 'signal', σ_g (high flow rate):

$$\sigma_{0,m} = a_0 + a_1\sigma_g. \tag{6}$$

When the ozone concentration is zero, $\sigma_{0,m} = \sigma_g = \sigma_0$, where σ_0 denotes the true baseline, so $a_0 = \sigma_0(1 - a_1)$. The expected response, equation (1), then becomes

$$\sigma_{0,m} - \sigma_g = \frac{(1 - a_1)aP}{1 + bP} \tag{7}$$

which is unaltered apart from a change in one of the fitting parameters.

Prediction of the ozone concentration from equation (7) is in practice problematic, because the 'zero' conductance can be very significantly larger than the 'signal' conductance and so the result can become very sensitively dependent on the accuracy of measurement of the 'zero'. Alternative prediction formulae using the sensor resistance, that are less sensitive to measurement errors but still preserve the drift correction idea embodied in equation (1), can be derived. As one example, if the measured 'zero' resistance is written $R_{0,m} = R_0 + \delta R$, where R_0 is a constant for any given sensor and the term δR includes both the variation with ozone concentration of the measured 'zero' and any variation over time due to baseline drifts, then

$$P = \frac{R_g - R_{0,m}}{aR_0R_g - b(R_g - R_{0,m})\left(1 - \dfrac{a\delta RR_g}{b(R_g - R_{0,m})}\right)}. \tag{8}$$

If $\frac{a\delta RR_g}{b(R_g - R_{0,m})}$ is sufficiently small, then the prediction function

$$P = \frac{R_g - R_{0,m}}{a'R_g - b(R_g - R_{0,m})} \tag{9}$$

with $a' = aR_0$ is implied. Figure 5 shows that this prediction function is robust against the variations in sensor characteristics.

3.2. Laboratory calibration results

As noted in the section on the calibration procedure, after the prediction (linearization) function is derived for each instrument and the fitting parameters are loaded, in a separate

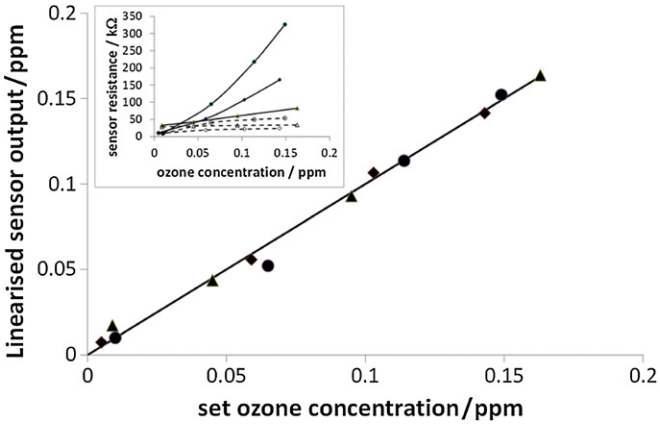

Figure 5. Example results of the linearization according to equation (9): three different low range sensors exemplifying results from devices within the lower, middle and upper quartiles of response, distinguished by different symbols. The line has unit slope. Inset: sensor resistance: closed symbols, high air flow rate ('signal'); open symbols, low air flow rate ('zero').

and independent calibration test, the resulting linearized output concentration is compared with ozone concentration determined by a reference analyser. An important question is whether there is any systematic bias introduced by the prediction function. Figure 6 shows the results of three-point calibrations for the linearized sensor heads, with linearized output predicting ozone analyser result, made over two different concentration ranges relevant to low-level ozone measurement, for over 3000 devices. The slope and intercept determined from the lowest and highest concentrations are uniformly and closely distributed around unity and zero respectively. The mid-range predictions are symmetrically and closely distributed around the actual value: there is no evidence for any bias such as might be caused by a systematic error in the linearization. The deviations closely fitted a normal distribution with standard deviation of the mid-range prediction ± 3 ppb at 70 ppb for the low-range instruments and ± 8 ppb at 120 ppb for the high-range instruments.

3.3. Validation through long-term measurement in the atmosphere

It has been shown that the observed long-term drifts of sensor conductance can largely be accounted for by drifts in the ozone-independent part of the conductance, and a rationalization has been offered [60]. If the 'zero ozone' conductance is continually checked then the signal drift can be compensated. This section presents demonstrations that the approach is robust in long-term measurement in the atmosphere.

3.3.1. Measurements alongside reference analysers in Houston, TX, USA. Figure 7 shows comparisons of hourly-averaged measurements from two ozone instruments alongside different reference analysers of the Texas Commission for Environmental Quality over a two month period in central Houston, USA. There is a small offset, which can be attributed to small differences in the calibration at these low ozone concentrations. There are some outliers, which can be traced to the effect of large short-term fluctuations in ozone concentration that are reflected differently in the hourly average from the different instruments. The long-term standard error of estimate of the semiconductor instrument predicting the reference analyser was less than 5 ppb.

3.3.2. Measurements in Auckland, NZ, with periodic ozone dosing. Previous preliminary reports of this work [56, 57] have shown long-term (60-day) standard error of estimate of semiconductor instrument predicting reference analyser of 2 ppb. These reports have also given a comparison of daily average ozone measurements for ten different instruments against a spectrometric analyser. In a trial lasting 70 days, daily average measurements were within ± 5 ppb for nine of the instruments. In one case, there was a significant drift, which was traced to a microstructure change on the sensor element and which is discussed further in the section on 'failure modes and their detection'.

3.3.3. Measurements in Rocky Mountain National Park, USA. In this case, the instruments were mounted in a remote area at an elevation of 2600 m during July–August 2010, without a nearby reference instrument. The comparison is therefore between two different instruments to determine whether there was any relative drift. The long-term (1100 h) standard error of estimate of the two instruments predicting one another was 0.6 ppb. The mean difference in measurements was 0.5 ppb.

3.3.4. Measurements in Sequoia and Kings Canyon National Parks (Ash Mountain), USA. A semiconductor-based instrument was co-located with a reference analyser operated by the US National Parks Service. The calibration was reconciled between the two instruments by correlating the readings over the first 48 h of operation. Figure 8 shows the initial correlation and then the difference in hourly average ozone between that predicted by the semiconductor instrument using the field calibration and that measured by the reference instrument. Long-term drift of the hourly averaged ozone concentration reported by the semiconductor instrument was less than 4 ppb in 1500 h. The standard deviation of prediction was 5 ppb, with ozone concentration ranging from 0 to 150 ppb. There was no significant drift of slope or offset of the correlation between the two instruments.

3.3.5. Measurements at an Environmental Protection Agency site close to an Interstate highway in Raleigh, NC, USA. Two semiconductor-based instruments were mounted alongside a reference site for a total period of four months, from October 2010 to January 2011. The calibration of the reference site was regularly checked. The semiconductor devices were not recalibrated. Figure 9(*a*) shows the correlation of hourly-averaged ozone measurement from the first 48 h of the trial and then for 48 h at the end of every month thereafter. The two semiconductor instruments match one another, and the correlation with the reference instrument was stable for the entire period. The regression slope relating semiconductor-indicated ozone to the reference analyser was not unity. This

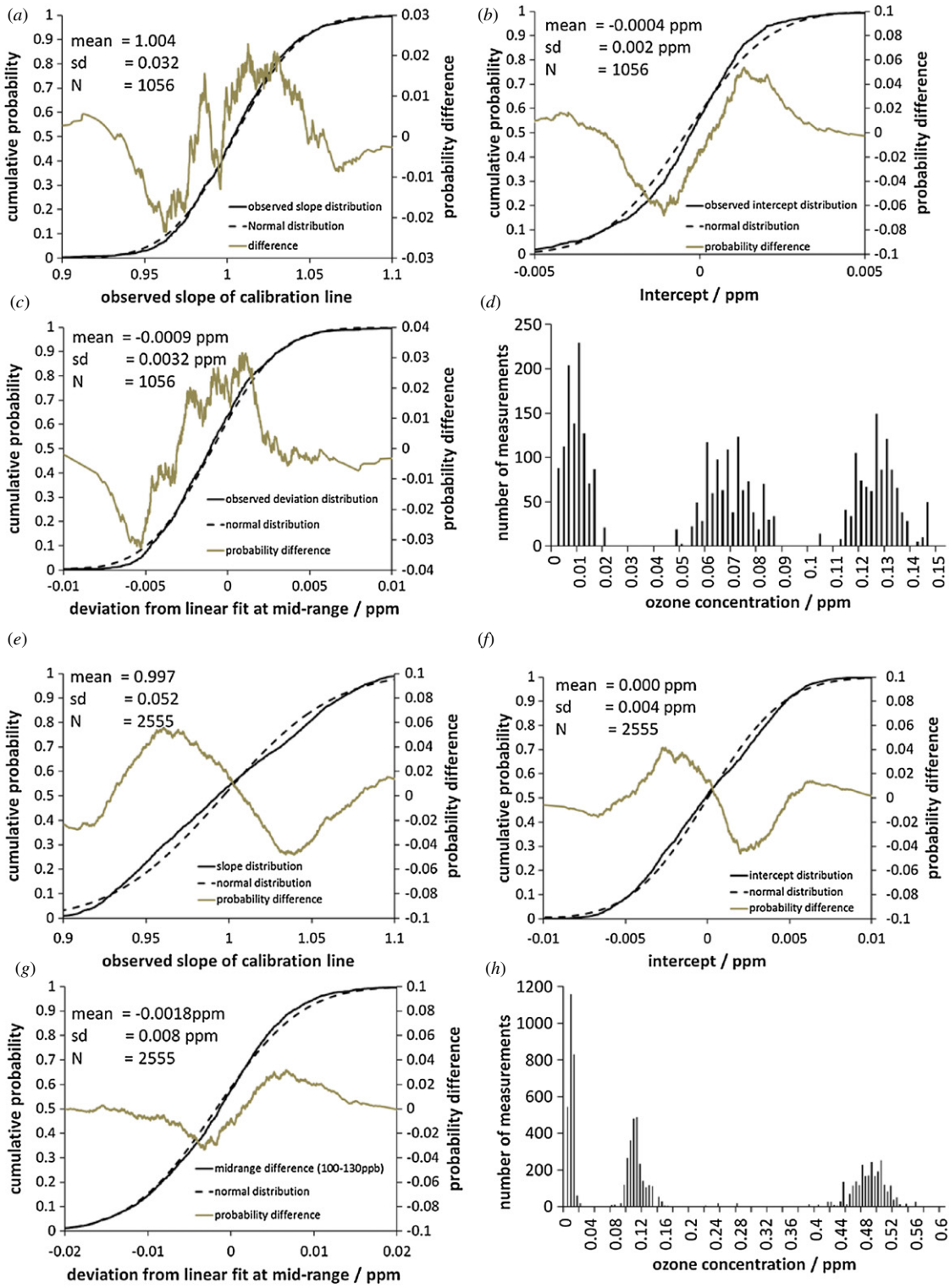

Figure 6. Three-point calibrations of linearized instruments, over two different ozone concentration ranges. (*a*), (*b*), (*e*), (*f*): slope and intercept derived from the end points; (*c*), (*g*): deviation of the mid-range point from the line defined by the end points; (*d*), (*h*): ozone concentration histograms for the measurements (*a*)–(*c*) and (*e*)–(*g*), respectively. Results for 1056 instruments calibrated over the 0–150 ppb range and 2555 different instruments calibrated over the 0–500 ppb range of ozone concentration in air. The observed distributions are compared with a normal distribution.

is not surprising and is traceable to errors of around $\pm 5\%$ in the measurements used for the linearization. Figure 9(*b*) shows the difference signal, with the semiconductor devices corrected by the correlation line obtained for 48 h at the beginning of the trial. There are many very short-term deviations but the overall trend confirms the stability. The two semiconductor devices remained stable against one another over the entire four months. Using the same reference calibration for both of them, derived from the beginning of the trial and shown in figure 9(*a*), the mean difference was 2.0 $\pm$ 1.6 ppb

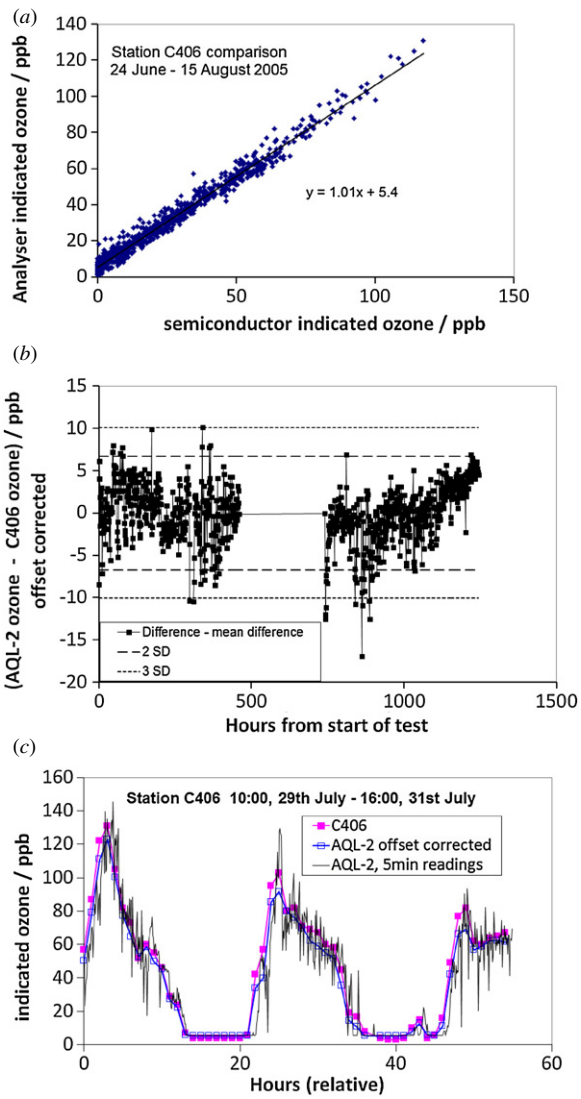

Figure 7. Comparison of semiconductor instrument (AQL-2) measurement with reference analyser (C406) measurements in central Houston, Texas, June-August 2005. Correlation of hourly average measurements (*a*) and time series of differences in hourly average measurements (*b*). Outliers are due to small differences in instrument timing leading to differences in averaging of short term fluctuations (*c*). Missing data are due to a period of extreme rain during which the semiconductor instruments, not being weatherproofed, were dismounted.

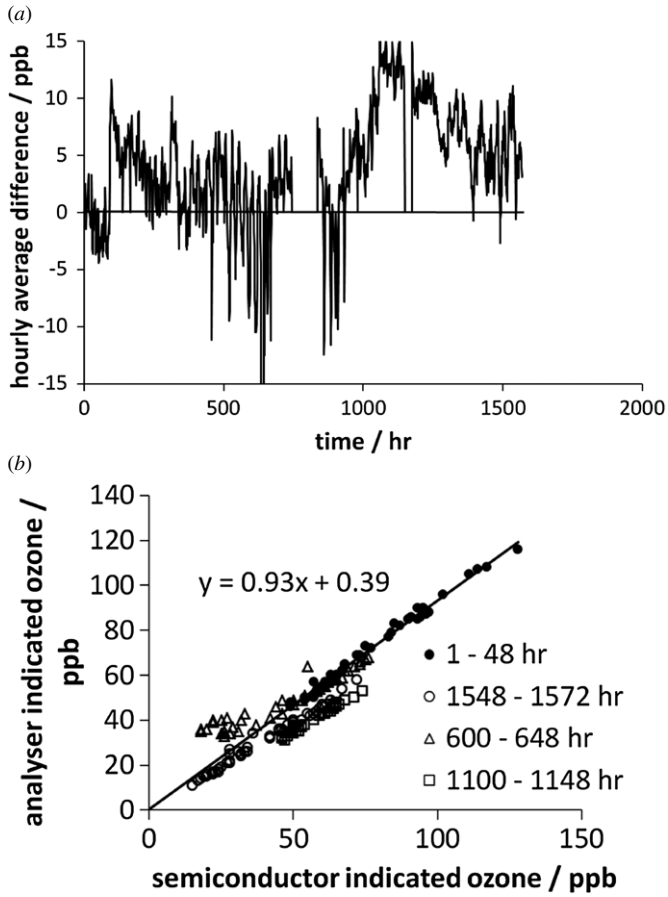

Figure 8. (*a*) Comparison of a semiconductor instrument with a reference analyser in Sequoia and Kings Canyon National Parks (Ash Mountain), USA, 27 August–31 October 2008. (*b*) Correlation of the first 48 h of measurements used to align the calibrations. Also shown are correlations from the end of the test and from the periods with the extremes of hourly average difference. Missing data are due to a software glitch.

and the short-term deviations observed in the comparison with the reference analyser were not present. This site was characterized by sudden ozone transients. Figure 9(*c*) shows one, occurring at around midnight at the end of October. The devices track one another and track the reference station except for a short period at the beginning of the transient. Such observations account for the short-term deviations in the difference: there are small differences in the clock timing between the semiconductor instruments and the reference station, and furthermore whilst both types of instrument measure every 1 min, the semiconductor instruments were configured to deliver 2 min averages and the reference station 5 min averages. When there are such large and sudden ozone transients these then cause single-point deviations in the hourly averages traceable to the slight misalignment of the clocks and the different averaging. Transients like this, occurring as they do in the night and thus without any ozone generation mechanism, are clearly a complex atmospheric phenomenon. The concentration of ozone near the highway is expected to be low in the dark, because ozone is scavenged by nitric oxide which is emitted from motor vehicles. However, when there is a stable nocturnal boundary layer, ozone generated as a result of photochemical reaction during the day can be stored higher in the troposphere. Then, it has been demonstrated that local and temporary weak turbulent instabilities in the nocturnal boundary layer near the ground can cause a local vertical mixing of the atmosphere, bringing ozone from above down to ground level [5, 64]. The transients detected here would appear to be an example of this phenomenon.

3.4. Failure modes and their detection

3.4.1. Dirty inlet tubes or filters. Ozone is an extremely reactive gas that decomposes readily on surfaces. It is important to use inlet tubes that are as wide and short as possible, made of an inert plastic like PTFE or of glass

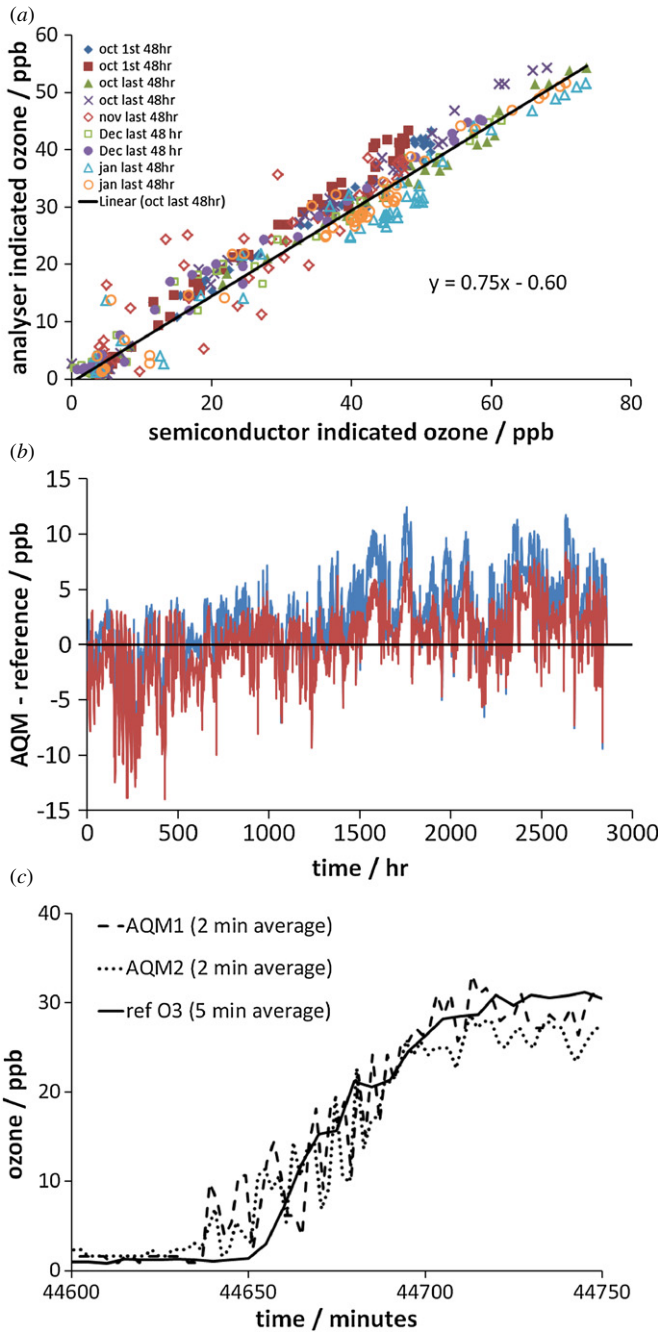

Figure 9. Four month comparison of two semiconductor-based instruments (AQM) with a reference station in Raleigh, North Carolina. (*a*) Correlation over successive 48 h periods of the hourly-averaged indicated ozone concentration. The correlation line is for one of the semiconductor devices, from a 48 h period at the beginning of the trial, and is used in (*b*) and (*c*) to correct both of the semiconductor device indications. (*b*) Difference of hourly average ozone reading. The different colours refer to the two different semiconductor instruments. (*c*) Typical sudden ozone transient (midnight, 31 October 2010).

or stainless steel or aluminium, and which are clean. The air also passes through a dust filter, which also keeps out droplets of water and which must be inert to ozone. For the semiconductor devices, the inlet tubes are necessarily small diameter. The inlet filters are of stainless steel mesh and porous PTFE. The volumetric flow rate of gas through the

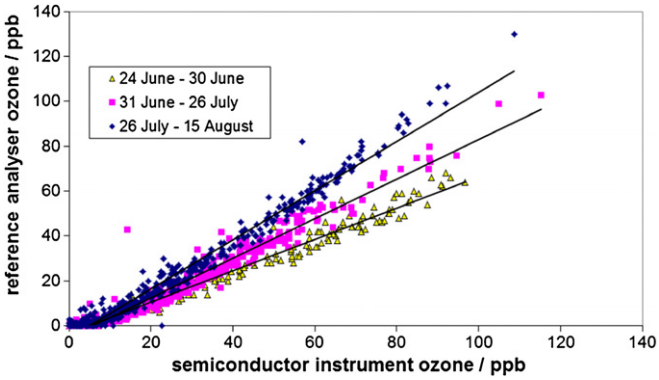

Figure 10. Comparison of a semiconductor instrument with reference analyser at a heavily industrialized site in Houston, USA. The progressive increase of slope is attributable to dirt accumulating on the inlet filter of the semiconductor instrument, causing it to register a lower ozone concentration for a given atmospheric concentration.

inlet is also necessarily low. As we have previously reported, accumulation of dirt on the inlet filters can cause a significant loss of ozone presented to the device [56]. Figure 10 shows an example, of a comparison between a semiconductor-based instrument and a reference analyser at a heavily polluted industrial site near the port of Houston, Texas. The calibration slope for the semiconductor device (semiconductor predicting reference instrument) increased over time, consistent with the ozone concentration presented to the sensor decreasing as a consequence of ozone decomposition on dirt deposited on the inlet filters and tubes. A simple optical reflection device could be used to report on the cleanliness of the filters, but this would increase the cost and complexity of the instrument overall.

3.4.2. Effects of sublimation of WO_3 from the sensing element in a humid atmosphere. At elevated temperature, in a humid atmosphere, tungstic oxide (the sensor material) can sublime. The result is that the sensor grows 'fur', as illustrated in figure 11. The effect is strongly dependent on the sensor temperature and hence is particularly affected by the high-temperature ('reset') part of the measurement cycle [56]. We have found that the effect can be minimized by careful adjustment of the temperature for this part of the cycle. The resultant effect is an increase both in the baseline (zero ozone) resistance of the sensor and an increase in the sensitivity to ozone. The occurrence of the effect can be detected by an increase in the sensor resistance measured during the low-flow, low-temperature ('baseline') part of the measurement cycle. The resultant increase in sensitivity is also observable through an increase in the ozone dependence of this 'baseline' measurement, which in turn is detectable by an increase in the magnitude of the diurnal oscillations of the 'baseline' caused by diurnal changes in ozone concentration. The effect is exemplified by results obtained during a study in the Lower Fraser Valley, Vancouver, Canada, illustrated in figure 11. The consequence of the failure is marked by the successive decrease of the calibration slope (semiconductor predicting reference instrument) and increase of the calibration intercept,

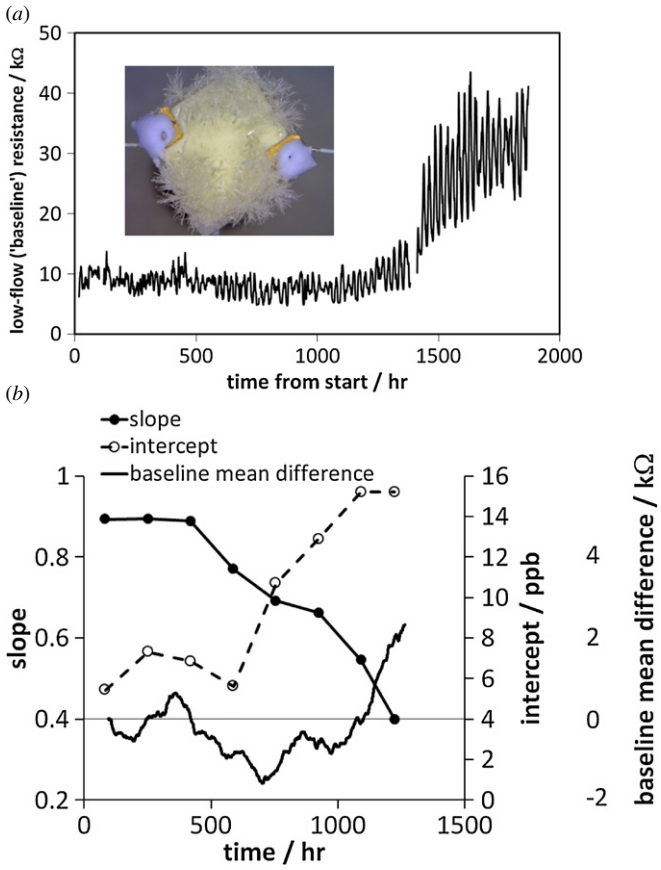

Figure 11. Illustration of a failure caused by sublimation of WO_3 from the sensor element (inset in (*a*), when the 'reset' temperature is too high. (*a*) The failure is indicated by a significant increase in the low-flow ('baseline') resistance of the sensor. (*b*) Change in sensor condition is detected by changes in the difference between a 96 h running mean and the cumulative mean baseline, and reflected in a change of apparent calibration slope and intercept-semiconductor instrument predicting co-located reference instrument.

here determined by a co-located reference instrument. One method for sensitively detecting the change is to compute the difference between the cumulative mean baseline resistance and a running mean baseline. A variation in this value from zero indicates a change in the condition of the sensor, which is reflected in the instrument indication. Figure 11 illustrates the point. In this case, there was a likely increase in the sensor temperature (indicated by the decrease in baseline resistance at about 500 h) followed by the sublimation effect (from about 900 h). The decrease in baseline resistance was marked by a decrease in apparent calibration slope but not a change in calibration intercept, effects which are consistent with an increase in sensor temperature. However, the sublimation effect resulted in such a large increase in both signal and baseline that the linearization algorithm failed, reflected in a drastic decrease in apparent calibration slope and increase in intercept.

3.4.3. Air pump failures. The performance of the semiconductor-based instrument is critically dependent on having a stable flow rate across the device. An outright pump failure is easily detected because the indicated ozone concentration falls immediately to zero. A more subtle failure is the effect of uncontrolled fluctuations in flow rate. The sensor itself can be helpful in detecting this occurrence, since it can function as a simple hot-wire anemometer. It is necessary only to measure the power dissipated from the heater by measuring the current through, and potential difference across, the heater track. Changes in this dissipation both in the high and low-temperature phases of the cycle reliably indicate pump failures and flow rate fluctuations [56].

4. Conclusion

We have demonstrated that simple, low-cost semiconductor-based instruments can provide reliable long-term measurement of atmospheric ozone, with performance that is close to that of reference analysers. Common failure modes for the devices have been elucidated and methods for detection of these failures using signals available from the sensors themselves have been described. Since the sensor, air pump and inlet filters are all contained in a small, replaceable housing which also holds sensor control electronics and the linearization and calibration information specific to that particular sensor, most maintenance simply comprises a change of this housing when a sensor, pump or filter failure is indicated. Maintenance costs are thereby also minimized. These instruments enable the economical construction and operation of ozone monitoring networks of accuracy, time resolution and spatial density sufficient to resolve the local gradients that are characteristic of urban air pollution.

Acknowledgments

This work was financially supported by the New Zealand Foundation for Research Science and Technology (Ministry of Business, Innovation and Employment), contract UOAX0709. We acknowledge considerable assistance in mounting field trials from: Greg Broyles, GHASP, Houston; Dr Nealson Watkins, US Environmental Protection Agency, Research Triangle Park, North Carolina; Dr John D Ray, US National Park Service, Air Resources Division, Denver, Colorado; Dr Ken Reid, MetroVancouver; Dr Bruce Ainslie, Environment Canada; Professor Ian McKendry and Professor Douw Steyn, University of British Columbia.

References

[1] Rao S *et al* 2012 Environmental modeling and methods for estimation of the global health impacts of air pollution *Environ. Model. Assess.* **17** 613–22

[2] Amann M *et al* 2008 *Health Risks of Ozone from Long-Range Trans-Boundary Air Pollution* (Copenhagen: World Health Organisation)

[3] Wang X K *et al* 2012 Effects of elevated O_3 concentration on winter wheat and rice yields in the Yangtze River Delta, China *Environ. Pollut.* **171** 118–25

[4] Smith G 2012 Ambient ozone injury to forest plants in Northeast and North Central USA: 16 years of biomonitoring *Environ. Monit. Assess.* **184** 4049–65

[5] Salmond J A and McKendry I G 2002 Secondary ozone maxima in a very stable nocturnal boundary layer: observations from the Lower Fraser Valley, BC *Atmos. Environ.* **36** 5771–82
[6] Castell-Balaguer N, Tellez L and Mantilla E 2012 Daily, seasonal and monthly variations in ozone levels recorded at the Turia river basin in Valencia (Eastern Spain) *Environ. Sci. Pollut. Res.* **19** 3461–80
[7] Adame J A, Lozano A, Bolivar J P, De la Morena B A, Contreras J and Godoy F 2008 Behavior, distribution and variability of surface ozone at an arid region in the south of Iberian Peninsula (Seville, Spain) *Chemosphere* **70** 841–9
[8] Ainslie B and Steyn D G 2007 Spatiotemporal trends in episodic ozone pollution in the Lower Fraser Valley, British Columbia, in relation to mesoscale atmospheric circulation patterns and emissions *J. Appl. Meteorol. Climatol.* **46** 1631–44
[9] Pires J C M, Sousa S I V, Pereira M C, Alvim-Ferraz M C M and Martins F G 2008 Management of air quality monitoring using principal component and cluster analysis - Part II: CO, NO_2 and O_3 *Atmos. Environ.* **42** 1261–74
[10] Rizzo M J and Scheff P A 2004 Assessing ozone networks using positive matrix factorization *Environ. Prog.* **23** 110–9
[11] Silva C and Quiroz A 2003 Optimization of the atmospheric pollution monitoring network at Santiago de Chile *Atmos. Environ.* **37** 2337–45
[12] Colvile R N, Hutchinson E J, Mindell J S and Warren R F 2001 The transport sector as a source of air pollution *Atmos. Environ.* **35** 1537–65
[13] Baldauf R W, Lane D D and Marote G A 2001 Ambient air quality monitoring network design for assessing human health impacts from exposures to airborne contaminants *Environ. Monit. Assess.* **66** 63–76
[14] Adams H S, Nieuwenhuijsen M J, Colvile R N, McMullen M A S and Khandelwal P 2001 Fine particle (PM2.5) personal exposure levels in transport microenvironments, London, UK *Sci. Total Environ.* **279** 29–44
[15] Gulliver J and Briggs D J 2004 Personal exposure to particulate air pollution in transport microenvironments *Atmos. Environ.* **38** 1–8
[16] Ching J and Majeed M A 2012 An approach to characterize within-grid concentration variability in air quality models *Atmos. Environ.* **49** 348–60
[17] Ainslie B, Reuten C, Steyn D G, Le N D and Zidek J V 2009 Application of an entropy-based Bayesian optimization technique to the redesign of an existing monitoring network for single air pollutants *J. Environ. Manage.* **90** 2715–29
[18] Strong J, Whyatt J D and Hewitt C N 2006 Application of multiple wind-roses to improve the modelling of ground-level ozone in the UK *Atmos. Environ.* **40** 7480–93
[19] McKendry I G, Steyn D G, Banta R M, Strapp W, Anlauf K and Pottier J 1998 Daytime photochemical pollutant transport over a tributary valley lake in Southwestern British Columbia *J. Appl. Meteorol.* **37** 393–404
[20] Thompson T M and Selin N E 2012 Influence of air quality model resolution on uncertainty associated with health impacts *Atmos. Chem. Phys.* **12** 9753–62
[21] Marshall J D, Brauer M and Frank L D 2009 Healthy neighborhoods: walkability and air pollution *Environ. Health Perspect.* **117** 1752–9
[22] Gulliver J and Briggs D J 2005 Time-space modeling of journey-time exposure to traffic-related air pollution using GIS *Environ. Res.* **97** 10–25
[23] Marshall J D, Nethery E and Brauer M 2008 Within-urban variability in ambient air pollution: comparison of estimation methods *Atmos. Environ.* **42** 1359–69
[24] Arain M A, Blair R, Finkelstein N, Brook J R, Sahsuvaroglu T, Beckerman B, Zhang L and Jerrett M 2007 The use of wind fields in a land use regression model to predict air pollution concentrations for health exposure studies *Atmos. Environ.* **41** 3453–64
[25] Su J G, Jerrett M and Beckerman B 2009 A distance-decay variable selection strategy for land use regression modeling of ambient air pollution exposures *Sci. Total Environ.* **407** 3890–8
[26] Su J G, Jerrett M, Beckerman B, Wilhelm M, Ghosh J K and Ritz B 2009 Predicting traffic-related air pollution in Los Angeles using a distance decay regression selection strategy *Environ. Res.* **109** 657–70
[27] Benvenuto F and Marani A 2000 Nowcasting of urban air pollutants by neural networks *Nuovo Cimento C; Geophys. Space Phys.* **23** 567–86
[28] Gardner M W and Dorling S R 1999 Neural network modelling and prediction of hourly NO_x and NO_2 concentrations in urban air in London *Atmos. Environ.* **33** 709–19
[29] Hasham F A, Kindzierski W B and Stanley S J 2004 Modeling of hourly NO_x concentrations using artificial neural networks *J. Environ. Eng. Sci.* **3** S111–9
[30] Munir S, Chen H B and Ropkins K 2012 Modelling the impact of road traffic on ground level ozone concentration using a quantile regression approach *Atmos. Environ.* **60** 283–91
[31] Carmichael G R, Sandu A, Chai T, Daescu D N, Constantinescu E M and Tang Y 2008 Predicting air quality: improvements through advanced methods to integrate models and measurements *J. Comput. Phys.* **227** 3540–71
[32] Fuentes M and Raftery A E 2005 Model evaluation and spatial interpolation by Bayesian combination of observations with outputs from numerical models *Biometrics* **61** 36–45
[33] Isakov V, Touma J S, Burke J, Lobdell D T, Palma T, Rosenbaum A and Ozkaynak H 2009 Combining regional- and local-scale air quality models with exposure models for use in environmental health studies *J. Air Waste Manage. Assoc.* **59** 461–72
[34] Sahu S K, Yip S and Holland D M 2009 Improved space-time forecasting of next day ozone concentrations in the eastern US *Atmos. Environ.* **43** 494–501
[35] van de Kassteele J and Stein A 2006 A model for external drift kriging with uncertain covariates applied to air quality measurements and dispersion model output *Environmetrics* **17** 309–22
[36] van de Kassteele J, Stein A, Dekkers A L M and Velders G J M 2009 External drift kriging of NO_x concentrations with dispersion model output in a reduced air quality monitoring network *Environ. Ecolog. Statist.* **16** 321–39
[37] van de Kassteele J and Velders G J M 2006 Uncertainty assessment of local NO_2 concentrations derived from error-in-variable external drift kriging and its relationship to the 2010 air quality standard *Atmos. Environ.* **40** 2583–95
[38] Yerramilli A *et al* 2011 Air quality modeling for the Urban Jackson, Mississippi region using a high resolution WRF/chem model *Int. J. Environ. Res. Public Health* **8** 2470–90
[39] Valari M and Menut L 2008 Does an increase in air quality models' resolution bring surface ozone concentrations closer to reality? *J. Atmos. Ocean. Technol.* **25** 1955–68
[40] Kanaroglou P S, Jerrett M, Morrison J, Beckerman B, Arain M A, Gilbert N L and Brook J R 2005 Establishing an air pollution monitoring network for intra-urban population exposure assessment: a location-allocation approach *Atmos. Environ.* **39** 2399–409
[41] Ainslie B, Steyn D G, Su J, Buzzelli M, Brauer M, Larson T and Rucker M 2008 A source area model incorporating simplified atmospheric dispersion and advection at fine

scale for population air pollutant exposure assessment *Atmos. Environ.* **42** 2394–404

[42] Mead M I *et al* 2013 The use of electrochemical sensors for monitoring urban air quality in low-cost, high-density networks *Atmos. Environ.* **70** 186–203

[43] Berry L and Brunet J 2008 Oxygen influence on the interaction mechanisms of ozone on SnO_2 sensors *Sensors Actuators* B **129** 450–8

[44] Contaret T, Seguin J L, Menini P and Aguir K 2013 Physical-based characterization of noise responses in metal-oxide gas sensors *IEEE Sens. J.* **13** 980–6

[45] Ghaddab B, Sanchez J B, Mavon C, Paillet M, Parret R, Zahab A A, Bantignies J L, Flaud V, Beche E and Berger F 2012 Detection of O_3 and NH_3 using hybrid tin dioxide/carbon nanotubes sensors: influence of materials and processing on sensor's sensitivity *Sensors Actuators* B **170** 67–74

[46] Guder F *et al* 2012 Superior functionality by design: selective ozone sensing realized by rationally constructed high-index ZnO surfaces *Small* **8** 3307–14

[47] Guerin J, Bendahan A and Aguir K 2008 A dynamic response model for the WO_3-based ozone sensors *Sensors Actuators* B **128** 462–7

[48] Kiriakidis G, Kortidis J, Moschovis K and Dovinos D 2008 On the road to inexpensive, sub-ppb, room temperature ozone detectors *Sens. Lett.* **6** 812–6

[49] Korotcenkov G and Cho B K 2012 Ozone measuring: what can limit application of SnO_2-based conductometric gas sensors? *Sensors Actuators* B **161** 28–44

[50] Korotcenkov G, Han S D, Cho B K and Brinzari V 2009 Grain size effects in sensor response of nanostructured SnO_2- and In_2O_3-based conductometric thin film gas sensor *Crit. Rev. Solid State Mater. Sci.* **34** 1–17

[51] Wu R J, Chen C Y, Chen M H and Sun Y L 2007 Photoreduction measurement of ozone using Pt/TiO_2-SnO_2 material at room temperature *Sensors Actuators* B **123** 1077–82

[52] Wu R J and Wu T M 2010 High sensor response and short response time of ozone sensor using Au/TiO_2-SnO_2 material at room temperature *Sensors Lett.* **8** 564–9

[53] Williams D E 1999 Semiconducting oxides as gas-sensitive resistors *Sensors Actuators* B **57** 1–16

[54] Williams D E, Aliwell S R, Pratt K F E, Caruana D J, Jones R L, Cox R A, Hansford G M and Halsall J 2002 Modelling the response of a tungsten oxide semiconductor as a gas sensor for the measurement of ozone *Meas. Sci. Technol.* **13** 923–31

[55] Williams D E, Henshaw G S, Wells D B, Ding G, Wagner J, Wright B, Yung Y F, Akagi J and Salmond J 2009 *35 Years of Chemical Sensors—an Honorary Symp. for Professor Jiri Janata's 70th Birthday Celebration* ed J Li *et al* (Pennington: Electrochemical Society Inc.) pp 251–4

[56] Williams D E, Henshaw G S, Wells D B, Ding G, Wagner J, Wright B E, Yung Y F and Salmond J A 2009 Development of low-cost ozone measurement instruments suitable for use in an air quality monitoring network *Chem. New Zealand* **73** 27–33

[57] Williams D E *et al* 2009 Development of low-cost ozone and nitrogen dioxide measurement instruments suitable for use in an air quality monitoring network *IEEE Sensors Conf. (Christchurch, New Zealand)* pp 1099–104

[58] Wang C Y, Becker R W, Passow T, Pletschen W, Kohler K, Cimalla V and Ambacher O 2011 Photon stimulated sensor based on indium oxide nanoparticles I: wide-concentration-range ozone monitoring in air *Sensors Actuators* B **152** 235–40

[59] Wang C Y *et al* 2007 Integration of In_2O_3 nanoparticle based ozone sensors with GaInN/GaN light emitting diodes *Appl. Phys. Lett.* **91** 103509

[60] Aliwell S R, Halsall J F, Pratt K F E, O'Sullivan J, Jones R L, Cox R A, Utembe S R, Hansford G M and Williams D E 2001 Ozone sensors based on WO_3: a model for sensor drift and a measurement correction method *Meas. Sci. Technol.* **12** 684–90

[61] Wilson J G, Kingham S, Pearce J and Sturman A P 2005 A review of intraurban variations in particulate air pollution: implications for epidemiological research *Atmos. Environ.* **39** 6444–62

[62] Utembe S R, Hansford G M, Sanderson M G, Freshwater R A, Pratt K F E, Williams D E, Cox R A and Jones R L 2006 An ozone monitoring instrument based on the tungsten trioxide (WO_3) semiconductor *Sensors Actuators* B **114** 507–12

[63] Hansford G M, Freshwater R A, Bosch R A, Cox R A, Jones R L, Pratt K F E and Williams D E 2005 A low cost instrument based on a solid state sensor for balloon-borne atmospheric O_3 profile sounding *J. Environ. Monit.* **7** 158–62

[64] Salmond J A and McKendry I G 2005 A review of turbulence in the very stable nocturnal boundary layer and its implications for air quality *Prog. Phys. Geogr.* **29** 171–88